Journal of Sound and Vibration (2001) **247**(3), 417–429
doi:10.1006/jsvi.2001.3748, available online at http://www.idealibrary.com on IDEAL®

DETERMINATION OF CRACK LOCATION IN BEAMS USING NATURAL FREQUENCIES

S. CHINCHALKAR

Department of Mechanical Engineering, Indian Institute of Technology, Bombay, Powai, Mumbai 400 076, *India. E-mail: chinch@me.iitb.ernet.in*

(*Received* 8 *June* 2000, *and in final form* 7 *December* 2000)

In this paper, we describe a numerical method for determining the location of a crack in a beam of varying depth when the lowest three natural frequencies of the cracked beam are known. The crack is modelled as a rotational spring and graphs of spring stiffness versus crack location are plotted for each natural frequency. The point of intersection of the three curves gives the location of the crack. Earlier work in this area involved the use of the Frobenius technique for solving the governing differential equation analytically and then using a semi-numerical approach to obtain the crack location. In this work, we use the finite element approach to solve the same problem. The beam is modelled using beam elements and the inverse problem of finding the spring stiffness, given the natural frequency, is shown to be related to the problem of a rank-one modification of an eigenvalue problem. Examples outlining the accuracy and ease of using this method are shown. The results are compared with those from semi-analytical approaches. The biggest advantage of this method is the generality in the approach; different boundary conditions and variations in the depth of the beam can be easily modelled.

1. INTRODUCTION

The detection of cracks in structures has received considerable attention lately and several techniques have been proposed. While the detection of cracks in complex structures is not a simple problem, the task of determining the location and size of a single crack in a beam is tractable. One of the techniques involves modelling the crack by a rotational spring [1, 2]. The forward problem is described as the problem of determination of the first few natural frequencies of the beam given the location and size of the crack. The inverse problem is described as the problem of determination of the location and the size of the crack given the first few natural frequencies of the cracked beam.

Nandwana and Maiti [1] and Chaudhari and Maiti [2] used a semi-analytical method for solving the forward as well as the inverse problem. For the forward problem, the governing differential equation for transverse vibration is written. The displacement solution can be written in terms of an infinite series and application of boundary conditions gives a characteristic equation whose roots yield the natural frequencies. To get numerical results, some computation is required. The infinite series cannot be summed analytically, so it is evaluated numerically using a certain number of terms. The characteristic equation is non-linear and needs to be solved using a root-finding algorithm. For certain beams, the computations give inaccurate results if standard double precision is used. Hence, quadruple precision calculations had to be performed. This has been reported in references [2, 3]. Also, for different boundary conditions and different variations in the depth of the beam (such as steps and tapers), the entire algebra has to be repeated, requiring considerable effort and expertise.

This is where a numerical approach is more suitable. In this paper, we have used a finite element based approach for solving the forward as well as inverse problems. The beam is

0022-460X/01/430417 + 13 $35.00/0

modelled using variable depth beam finite elements with two nodes and two degrees of freedom (d.o.f.) per node. As in the semi-analytical approach, the crack is modelled by a rotational spring. The forward problem then reduces to the solution of a generalized eigenvalue problem, which can be solved accurately using double precision. Different boundary conditions can also be modelled easily.

The inverse problem involves determination of the crack location and size given the first three natural frequencies of the cracked beam. In the semi-analytical approach, different locations of the crack are tried out. For each location, the characteristic equation now contains the unknown stiffness of the spring. However, the natural frequency is now known. Thus, the stiffness of the spring which results in the given natural frequency can be determined. This is done for all three natural frequencies and graphs of spring stiffness versus crack location are obtained. Since physically there is only one crack, the intersection of the three curves gives the crack location. The crack size is obtained from the spring stiffness using another relation. Again, for different variations in depth of the beam as well as for different boundary conditions, the algebra has to be repeated and it requires considerable effort.

Here, we use a numerical approach for the inverse problem as well. We first solve a 'nearby' forward problem of determining the first three natural frequencies of a beam with crack modelled as a rotational spring of zero stiffness. While this does not correspond to any physical system, it directly leads us to the solution of the inverse problem. The introduction of a spring of an unknown stiffness can be shown to be equivalent to a rank-one modification of an eigenvalue problem whose lowest three eigenvalues are known. The unknown stiffness can be easily and efficiently solved for. This is repeated for different crack locations as in the semi-analytical method and graphs of spring stiffness versus crack location are obtained.

The rest of the paper is organized as follows. In section 2, we outline the basic finite element approach for finding the natural frequencies of a beam. In section 3, we use the finite element approach for computing the natural frequencies of truncated wedge beams with different boundary conditions. The results are compared with those given in reference [3] and are found to be sufficiently accurate. In section 4, the inverse problem is modelled as a rank-one modification of an eigenvalue problem. In section 5, we present numerical examples which compare this method with the semi-analytical method used in references [1, 2].

2. THE FINITE ELEMENT FORMULATION

Figure 1 shows a single beam element with two nodes. It has two d.o.f. at each node, the transverse deflection, v, and the rotation, $\theta = \mathrm{d}v/\mathrm{d}x$. This is the same as the standard beam element except for the fact that the depth, $h(x)$, is a function of x. We have assumed a linear variation from h_1 at the left end to h_2 at the right end. We use the shape functions for a uniform beam to model the displacement in this beam element. These shape functions are given by [4]

$$\mathbf{N} = \begin{Bmatrix} 1 - 3\left(\dfrac{x}{L}\right)^2 + 2\left(\dfrac{x}{L}\right)^3 \\ x\left(1 - \left(\dfrac{x}{L}\right)\right)^2 \\ 3\left(\dfrac{x}{L}\right)^2 - 2\left(\dfrac{x}{L}\right)^3 \\ x\left(\left(\dfrac{x}{L}\right)^2 - \left(\dfrac{x}{L}\right)\right) \end{Bmatrix}, \tag{1}$$

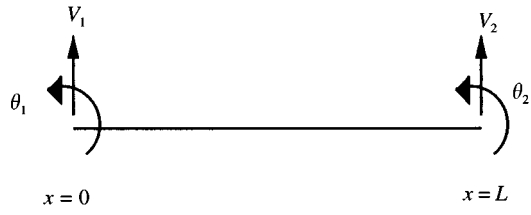

Figure 1. A single beam element of length l.

where L is the length of the beam element. The element stiffness matrix and the consistent element mass matrix are given by

$$\mathbf{K}_e = \int_0^L \frac{\mathrm{d}^2\mathbf{N}}{\mathrm{d}x^2} EI(x) \frac{\mathrm{d}^2\mathbf{N}^{\mathrm{T}}}{\mathrm{d}x^2} \mathrm{d}x, \tag{2}$$

$$\mathbf{M}_e = \int_0^L \mathbf{N}\mathbf{N}^{\mathrm{T}} \rho A(x) \mathrm{d}x, \tag{3}$$

where

$$h(x) = h_1 + \frac{h_2 - h_1}{L} x, \tag{4}$$

$$A(x) = bh(x), \tag{5}$$

$$I(x) = \frac{bh(x)^3}{12}, \tag{6}$$

where b is the (uniform) width of the beam, E is Young's modulus, ρ is the density, $A(x)$ is the area of the cross-section of the beam at a distance x from the left node, and $I(x)$ is the cross-sectional moment of inertia at a distance x from the left node.

The integrand for $\mathbf{K}_e$ will contain fifth order terms in x and the integrand for $\mathbf{M}_e$ will contain seventh order terms in x. Both integrals can be evaluated exactly using a four-point Gaussian quadrature. The mass and stiffness matrices are assembled as usual. Boundary conditions can be of the following types.

$$\text{Clamped:} \quad v = 0, \quad \theta = 0, \tag{7}$$

$$\text{Pinned:} \quad v = 0, \tag{8}$$

$$\text{Sliding:} \quad \theta = 0, \tag{9}$$

$$\text{Free:} \quad \text{no restriction on } v \text{ or } \theta. \tag{10}$$

Those d.o.f.s that are set to zero due to boundary conditions are eliminated from the equations and we are left with a generalized eigenvalue problem

$$\mathbf{K}^{(g)}\mathbf{u} = \lambda \mathbf{M}^{(g)}\mathbf{u}, \tag{11}$$

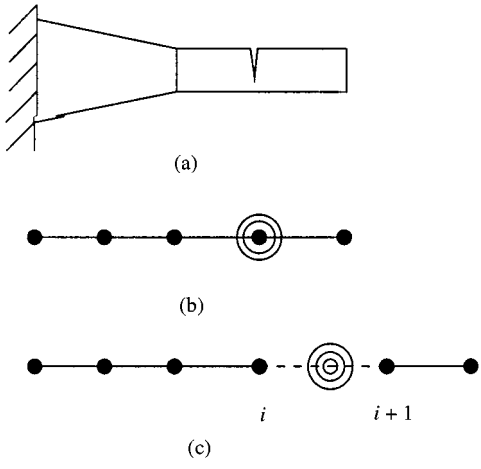

Figure 2. (a) Beam with crack; (b) a sample discretization using beam elements and (c) an 'expanded' view of the discretization.

where $\mathbf{K}^{(g)}$ and $\mathbf{M}^{(g)}$ are, respectively, the global stiffness and mass matrices and u is the vector of unknown nodal d.o.f.s. The eigenvalues, λ, are the squares of the natural frequencies and can be computed using any standard generalized eigensolver.

For computational convenience, we have used a lumped mass matrix instead of the above consistent mass matrix. Lumping is done by scaling the diagonal entries of the mass matrix such that the total mass is conserved, and zeroing out all off-diagonal entries. This results in substantial savings in computational effort in solving the eigenvalue problem with only a small adverse effect on accuracy. Details can be found in Cook [5]. Using this diagonal lumped mass matrix, $\mathbf{M}$, instead of $\mathbf{M}^{(g)}$, the generalized eigenvalue problem can be reduced to the standard eigenvalue problem in the following manner. Premultiplying both sides of equation (11) by $\mathbf{M}^{-1/2}$ and using the fact that $\mathbf{M}^{-1/2}\mathbf{M}^{1/2}$ is the identity matrix we get

$$\mathbf{M}^{-1/2}\mathbf{K}^{(g)}\mathbf{M}^{-1/2}\mathbf{M}^{1/2}\mathbf{u} = \lambda\mathbf{M}^{1/2}\mathbf{u} \tag{12}$$

which simplifies to

$$\mathbf{A}\mathbf{d} = \lambda\mathbf{d}, \tag{13}$$

where

$$\mathbf{A} = \mathbf{M}^{-1/2}\mathbf{K}^{(g)}\mathbf{M}^{-1/2}, \tag{14}$$

$$\mathbf{d} = \mathbf{M}^{1/2}\mathbf{u}. \tag{15}$$

The shape functions do not capture the mode shapes of the beam and hence the solution is approximate. By increasing the number of elements, the accuracy can be increased.

We now move on to the forward problem of determining the natural frequencies of a beam with a crack, given the location and size of the crack. A transverse crack in a beam can be represented by a torsional spring (see references [1, 2]) as shown in Figure 2. Suppose we know the stiffness, k, of the spring and want to compute the natural frequencies. The above formulation can be extended to this case. Figure 2c shows an 'expanded' view of the

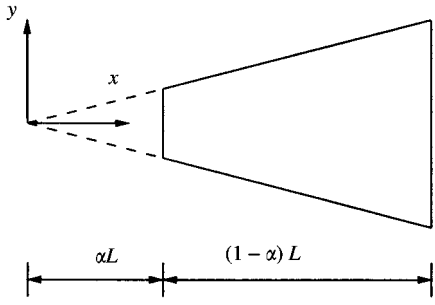

Figure 3. A wedge beam with truncation factor α [3].

beam in Figure 2b. The spring connects nodes i and $i + 1$ and couples the rotations, θ_i and θ_{i+1} through the stiffness matrix

$$\mathbf{K}_s = \begin{bmatrix} k & -k \\ -k & k \end{bmatrix}. \tag{16}$$

Additionally, the vertical deflection of nodes i and $i + 1$ are the same, i.e., $v_i = v_{i+1}$. This can be easily accounted for by representing the vertical deflection of both nodes i and $i + 1$ by a single d.o.f. This stiffness matrix, $\mathbf{K}_s$, is also assembled into the global stiffness matrix, $\mathbf{K}^{(g)}$. The solution of the eigenvalue problem can then proceed as usual.

3. NATURAL FREQUENCIES OF TRUNCATED WEDGE BEAMS

Since the forward problem involves the determination of the natural frequencies of a cracked beam given the location and size of the crack, as a first step, we will determine the natural frequencies of an uncracked wedge beam using FEM and compare the results with those obtained by Naguleswaran [3].

Figure 3 shows a truncated wedge beam whose natural frequencies are to be determined. Using the notation from Naguleswaran [3], we denote the truncation factor by α and the modified dimensionless natural frequency by Ω_m, where

$$\Omega_m^2 = (1 - \alpha)^4 m(L)\omega^2 L^4 / EI(L), \tag{17}$$

where $m(L)$ is the mass per unit length at $x = L$, $EI(L)$ is the flexural rigidity at $x = L$, and ω is the natural frequency in rad/s.

Naguleswaran [3] calculated the first three modified dimensionless natural frequencies for beams with different boundary conditions and truncation factors using the method of Frobenius. This is a semi-analytical method which involves expressing the deflection of the beam by a power series, retaining sufficient terms, and iteratively finding roots of a non-linear equation to obtain the natural frequencies.

By discretizing the beam into 50 elements of equal length and using the method outlined in section 2, the first three modified dimensionless natural frequencies, Ω_{m1}, Ω_{m2}, Ω_{m3}, were determined. Table 1 compares the first three natural frequencies computed using the FEM approach and the Frobenius method for clamped–clamped (cl–cl) and pinned–sliding (pn–sl) beams for different truncation factors, α. In the table, an asterisk (*) indicates that the computation of the frequency for the same mode for higher truncation factors requires

TABLE 1

A comparison of semi-analytical and FEM results for wedge beams

α		cl–cl [3]	cl–cl FEM	pn–sl [3]	pn–sl FEM
0·05	Ω_{m1}	8·6237	8·6239	1·0962	1·0962
	Ω_{m2}	23·4919	23·4910	9·7820	9·7817
	Ω_{m3}	45·7416	45·7358	25·3493	25·3469
0·10	Ω_{m1}	9·8846	9·8844	1·2841	1·2841
	Ω_{m2}	27·0084	27·0067	10·8970	10·8967
	Ω_{m3}	52·7080	52·7002	28·5479	28·5452
0·15	Ω_{m1}	10·9209	10·9207	1·4230	1·4230
	Ω_{m2}	29·9041	29·9022	11·8083	11·8080
	Ω_{m3}	58·4341	58·4257	31·2153	31·2125
0·20	Ω_{m1}	11·8417	11·8415	1·5372	1·5372
	Ω_{m2}	32·4755	32·4734	12·6181	12·6178
	Ω_{m3}	*63·5118	63·5029	33·6057	33·6028
0·25	Ω_{m1}	12·6886	12·6884	1·6357	1·6357
	Ω_{m2}	34·8384	34·8362	13·3648	13·3645
	Ω_{m3}	68·1728	68·1635	35·8181	35·8151
0·30	Ω_{m1}	13·4832	13·4830	1·7231	1·7231
	Ω_{m2}	*37·0527	37·0504	14·0679	14·0675
	Ω_{m3}	72·5368	72·5271	37·9036	37·9005
0·35	Ω_{m1}	14·2381	14·2379	1·8021	1·8021
	Ω_{m2}	39·1539	39·1515	14·7387	14·7383
	Ω_{m3}	76·6753	76·6651	*39·8927	39·8895
0·40	Ω_{m1}	14·9616	14·9613	1·8744	1·8744
	Ω_{m2}	41·1656	41·1631	15·3845	15·3841
	Ω_{m3}	80·6348	80·6242	41·8053	41·8020
0·45	Ω_{m1}	*15·6593	15·6591	1·9411	1·9411
	Ω_{m2}	43·1039	43·1013	16·0103	16·0099
	Ω_{m3}	84·4478	84·4368	43·6555	43·6521
0·50	Ω_{m1}	16·3356	16·3353	2·0033	2·0033
	Ω_{m2}	44·9806	44·9779	*16·6199	16·6194
	Ω_{m3}	88·1389	88·1268	45·4535	45·4499
0·55	Ω_{m1}	16·9935	16·9932	2·0615	2·0615
	Ω_{m2}	46·8049	46·8021	17·2158	17·2153
	Ω_{m3}	—	91·7120	47·2069	47·2032
0·60	Ω_{m1}	17·6354	17·6351	2·1162	2·1162
	Ω_{m2}	48·5839	48·5807	17·8002	17·7997
	Ω_{m3}	—	95·2063	48·9218	48·9180
0·65	Ω_{m1}	18·2634	18·2631	2·1679	2·1679
	Ω_{m2}	—	50·3193	18·3747	18·3742
	Ω_{m3}	—	98·6210	—	50·5990
0·70	Ω_{m1}	18·8791	18·8788	*2·2169	2·2169
	Ω_{m2}	—	52·0225	18·9407	18·9402
	Ω_{m3}	—	101·9649	—	52·2502

quadruple precision computation, as in table 1 indicates unacceptably inaccurate results even with quadruple precision computation. Several things are evident from this table. First, the FEM results are approximately within 0·01 per cent of the analytical results and are considered accurate enough for the computations that follow. Second, the FEM results for all values of α were generated using double precision calculations with no deterioration in accuracy. Third, even for large values of α, when the Frobenius method failed to give an acceptable answer, the FEM results appear to be correct, although no independent confirmation can be obtained because of lack of data. Fourth, different end conditions such as clamped, pinned, or free could be handled using the same program merely by changing the boundary conditions in a data file.

4. THE INVERSE PROBLEM

We now consider the numerical solution of the inverse problem of determination of crack location given the first three natural frequencies. As in the case of the semi-analytical approach, we try out different locations of the crack, insert a torsional spring in our FE model, and determine the value of the spring stiffness which gives rise to the frequency equal to the measured value. Consider Figure 2 again. We will first solve our real symmetric eigenvalue problem, $\mathbf{Ad} = \lambda\mathbf{d}$, with the spring stiffness set to zero. Note that this is different from not having a spring at all. The vertical displacements of nodes i and $i+1$ are the same, but the slopes, θ_i and θ_{i+1}, are unrelated. While this may have no physical significance, it will help us solve the inverse problem.

Suppose we have solved the eigenvalue problem with a spring of zero stiffness and obtained the eigenvalues, $\mathbf{\Lambda}$, and the eigenvectors, $\mathbf{Q}$, so that

$$\mathbf{Q}^{\mathrm{T}}\mathbf{A}\mathbf{Q} = \mathbf{\Lambda}. \tag{18}$$

Here, $\mathbf{\Lambda}$ is a diagonal matrix of eigenvalues of $\mathbf{A}$ and $\mathbf{Q}$ is an orthonormal matrix whose columns are the eigenvectors of $\mathbf{A}$. That is

$$\mathbf{\Lambda} = \begin{bmatrix} \lambda_1 & & \\ & \ddots & \\ & & \lambda_n \end{bmatrix}, \qquad \mathbf{Q}\mathbf{Q}^{\mathrm{T}} = \mathbf{Q}^{\mathrm{T}}\mathbf{Q} = \mathbf{I}. \tag{19}$$

When we insert a torsional spring of (unknown) stiffness, k, the matrix $\mathbf{A}$ changes to $\bar{\mathbf{A}} = \mathbf{A} + \mathbf{M}^{-1/2}\bar{\mathbf{K}}\mathbf{M}^{-1/2}$ where $\bar{\mathbf{K}}$ is a matrix of the same size as $\mathbf{A}$ and mostly zero, except that it contains the submatrix $\mathbf{K}_s$ (given in equation (16)) at the appropriate location. More precisely, if θ_i is d.o.f. j and θ_{i+1} is d.o.f. $j+1$, then $\bar{\mathbf{K}}(j, j) = k$, $\bar{\mathbf{K}}(j, j+1) = -k$, $\bar{\mathbf{K}}(j+1, j) = -k$, and $\bar{\mathbf{K}}(j+1, j+1) = k$ are the only non-zero elements of $\bar{\mathbf{K}}$. $\bar{\mathbf{K}}$ is a rank-one matrix given by

$$\bar{\mathbf{K}} = k\bar{z}\bar{z}^{\mathrm{T}}, \tag{20}$$

where $\bar{z} = \{0, \ldots, 0, 1, -1, 0, \ldots, 0\}^{\mathrm{T}}$. Hence, the matrix $\bar{\mathbf{A}}$ can also be written as a rank-one modification of $\mathbf{A}$ as follows:

$$\bar{\mathbf{A}} = \mathbf{A} + k\mathbf{z}\mathbf{z}^{\mathrm{T}}, \tag{21}$$

where $\mathbf{z} = \mathbf{M}^{-1/2}\bar{\mathbf{z}}$ can be computed easily. So our inverse problem is now reduced to finding the value of k such that a given value, say $\bar{\lambda}$, is an eigenvalue of $\bar{\mathbf{A}}$. By using a similarity transformation (since $\mathbf{Q}$ is orthonormal, $\mathbf{Q}^{-1} = \mathbf{Q}^{\mathrm{T}}$), the above equation can be transformed into

$$\mathbf{Q}^{\mathrm{T}}\bar{\mathbf{A}}\mathbf{Q} = \mathbf{Q}^{\mathrm{T}}\mathbf{A}\mathbf{Q} + k\mathbf{Q}^{\mathrm{T}}\mathbf{z}\mathbf{z}^{\mathrm{T}}\mathbf{Q} \tag{22}$$

$$= \mathbf{\Lambda} + k\mathbf{w}\mathbf{w}^{\mathrm{T}}, \tag{23}$$

where $\mathbf{w} = \mathbf{Q}^{\mathrm{T}}\mathbf{z}$. We already know $\mathbf{\Lambda}$, and $\mathbf{w}$ can be computed easily as $\mathbf{Q}$ and $\mathbf{z}$ are known. Again, note that equation (23) involves a rank-one modification of a known matrix, $\mathbf{\Lambda}$. Also note that if $\bar{\lambda}$ is an eigenvalue of $\bar{\mathbf{A}}$, then it is also an eigenvalue of $\mathbf{Q}^{\mathrm{T}}\bar{\mathbf{A}}\mathbf{Q}$ since eigenvalues are not changed by similarity transformations. From the definition of eigenvalues, $p(\bar{\lambda}) = \det(\mathbf{\Lambda} + k\mathbf{w}\mathbf{w}^{\mathrm{T}} - \bar{\lambda}\mathbf{I}) = 0$. The following simple algorithm calculates $p(\bar{\lambda})$ given $\bar{\lambda}$ (see reference [6] for details).

$r_1(\bar{\lambda}) = 1,$

$p_1(\bar{\lambda}) = (\lambda_1 - \bar{\lambda}) + kw_1^2$

for $i = 2$ to n,

$r_i(\bar{\lambda}) = (\lambda_{i-1} - \bar{\lambda})r_{i-1}(\bar{\lambda}),$

$p_i(\bar{\lambda}) = (\lambda_i - \bar{\lambda})p_{i-1}(\bar{\lambda}) + kw_i^2 r_i(\bar{\lambda})$

end

$p(\bar{\lambda}) = p_n(\bar{\lambda}).$

In our case, we now that $p(\bar{\lambda}) = 0$, but we do not know k. However, since $p(\bar{\lambda})$ is a linear function of k, it is quite trivial to rewrite the above algorithm to give us k knowing that $p(\bar{\lambda}) = 0$ as follows:

$r_1 = 1,$

$b_1 = \lambda_1 - \bar{\lambda},$

$c_1 = w_1^2$

for $i = 2$ to n,

$r_i = (\lambda_{i-1} - \bar{\lambda})r_{i-1},$

$b_i = (\lambda_i - \bar{\lambda})b_{i-1},$

$c_i = w_i^2 r_i + (\lambda_i - \bar{\lambda})c_{i-1}$

end

$k = -b_n/c_n.$

r_i, b_i, c_i can become very large and hence their mantissas and exponents must be stored separately. The above algorithm has to be executed once for each value of the measured natural frequency, $\bar{\lambda}$, to obtain the three values of spring stiffness. This has to be repeated at several different locations along the length of the beam; the nodes provide convenient locations for inserting a spring.

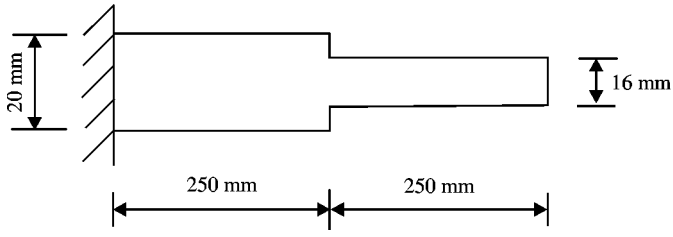

Figure 4. A two-segment beam [1].

TABLE 2

Different crack locations and sizes along with the FE-based natural frequencies used in this study [1]

Case number	Crack position $\beta^* = x/L$	Crack size a/h	Natural frequencies (rad/s)		
			ω_1	ω_2	ω_3
	Uncracked	Uncracked	455·0	2345·9	6506·7
1	0·05	0·10	451·5	2334·0	6483·7
2	0·20	0·10	453·0	2345·7	6498·4
3	0·40	0·10	454·2	2341·6	6488·3
4	0·45	0·10	454·4	2340·1	6499·4
5	0·20	0·20	477·6	2344·6	6480·9
6	0·20	0·30	438·3	2342·7	6448·3
7	0·20	0·40	423·8	2339·7	6398·3
8	0·20	0·50	402·2	2335·5	6323·1

For each of the three measured natural frequencies, we plot a graph of stiffness, k, versus crack location. Since there is only one crack, the point of intersection of the three curves gives us the crack location. In most cases, however, the three curves do not intersect because of inaccuracies in the modelling as compared to measured results. For this purpose, the 'zero-setting' procedure described in references [1, 7] is used. In this procedure, Young's modulus of the beam is changed, so that the measured natural frequencies of the uncracked beam match the computed natural frequencies of the uncracked beam. For each frequency, a different Young's modulus may have to be used. This is some sort of a 'scaling' to reduce the effect of modelling errors. The next section describes the results obtained for several test cases.

5. NUMERICAL EXAMPLES

The first example comes from reference [1]. All input values are as given in that paper. Figure 4 shows a stepped beam with material data as follows: Young's modulus = $2{\cdot}1 \times 10^{11}$ N/m^2, density = 7800 kg/m^3, and the Poisson ratio = 0·3. Table 2 shows crack locations and sizes and corresponding 'measured' natural frequencies. These frequencies were obtained in reference [1] by performing a finite element analysis with a very fine mesh. For comparison with that paper, we plot non-dimensional stiffness, $K = kL/EI_1$ versus crack location $\beta = x/L$ for different natural frequencies. L is the length of the beam

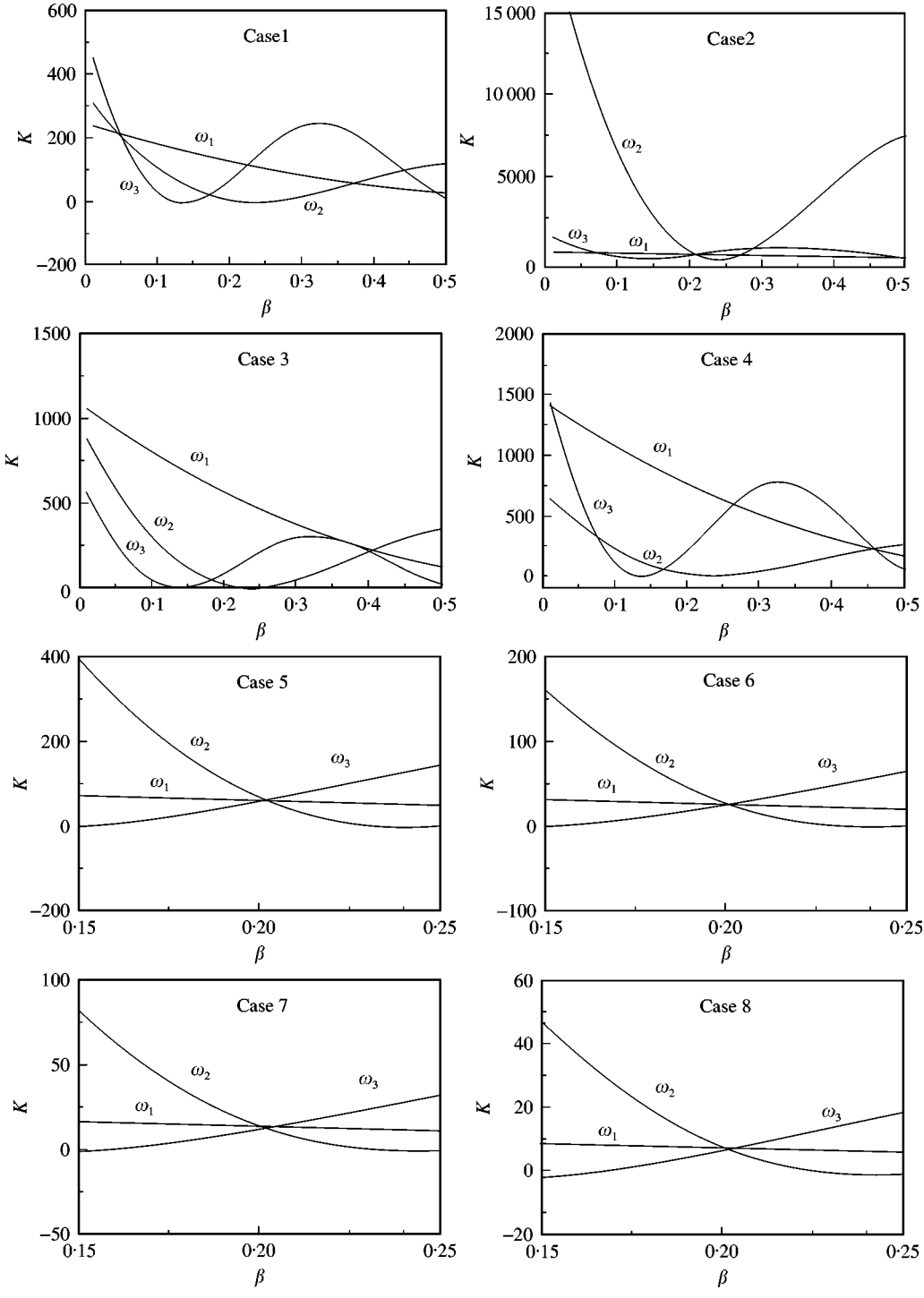

Figure 5. Variation of spring stiffness with location for test cases from reference [1].

(500 mm), E is Young's modulus, and I_1 is the cross-sectional moment of inertia of the left section of the beam. Figure 5 shows these plots. A comparison with reference [1] shows that they are essentially identical. Table 3 shows the results in a tabular form. The error in crack

TABLE 3

Comparison of results obtained by numerical method with results in reference [1]

Case number	Actual crack location β^*	Predicted location	
		β^* [1]	β^* (FEM)
1	0·05	0·0494	0·0481
2	0·20	0·2061	0·2098
3	0·40	0·4028	0·3980
4	0·45	0·4583	0·4578
5	0·20	0·2013	0·2020
6	0·20	0·2004	0·2010
7	0·20	0·2001	0·2004
8	0·20	0·2002	0·2005

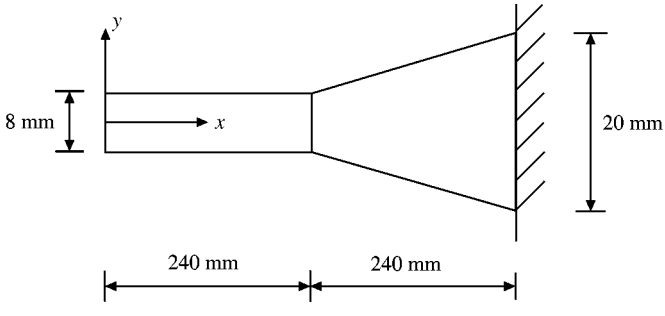

Figure 6. A two-segment beam with one tapered segment [2].

TABLE 4

Comparison of actual and predicted crack locations

Actual		Natural frequencies (Hz) [2]			Predicted location	
Location β^*	Size a (mm)	ω_1	ω_2	ω_3	β [2]	β (FEM)
Uncracked	Uncracked	61·18	275·11	686·81		
0·4	3·0	60·39	268·78	685·11	0·390	0·395
0·8	4·51	60·11	271·38	686·09	0·83	0·806

location is roughly similar to that in reference [1]. This is to be expected as the numerical method approaches the problem in a manner almost identical to the semi-analytical approach.

The next example is from reference [2]. Figure 6 shows a two-segment beam with one uniform and one tapered section. As in reference [2], the following input values were chosen: length = 480 mm, width = 12 mm, depth at the fixed end = 20 mm, depth at free end = 8 mm, length of taper section = 240 mm and length of uniform section = 240 mm. The density Young's modulus, and the Poisson ratio are as in the previous example. Table 4 shows the crack locations and sizes and the natural frequencies obtained by FEM. Using this data, and the above numerical approach, the variation of non-dimensional stiffness,

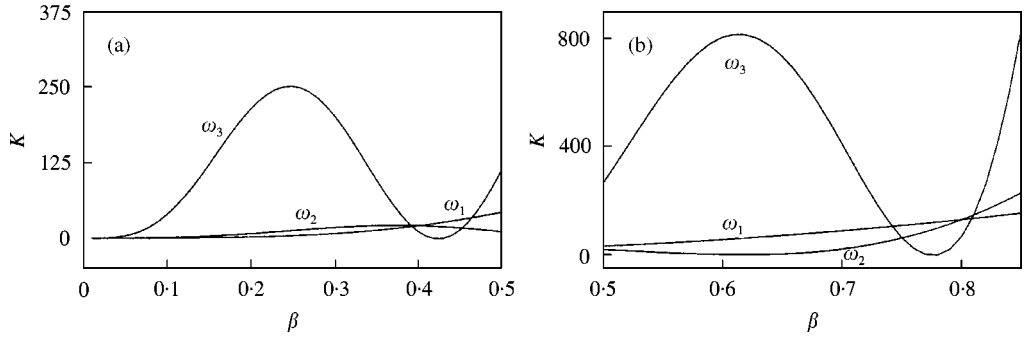

Figure 7. Variation of spring stiffness with location for test cases from reference [2]. Crack location: (a) $\beta^* = 0{\cdot}4$, $a = 3$ mm; (b) $\beta^* = 0{\cdot}8$, $a = 4{\cdot}51$ mm.

$K = kL_1/EI_1$, versus crack location as shown in Figure 7 was obtained. Here, L_1 is the length of the uniform section of the beam, (240 mm), E is Young's modulus, and I_1 is the cross-sectional moment of inertia of the uniform portion of the beam. The results are presented in the last column in Table 4. Again, a comparison with reference [2] shows that the results are almost as accurate as the semi-analytical results.

For all the above test cases, 100 elements of equal length were used to discretize the beam. For each case, the execution time of the program was just under 1 min on a 400 MHz Pentium-II computer. Since this was a reasonably small amount of time, further improvements in computational speed were considered unnecessary.

In most cases, because of numerical inaccuracies, the three curves did not intersect precisely at a single point. Therefore, the centroid of the triangle formed by the intersection of the three curves was taken as the point of intersection.

6. DISCUSSION AND CONCLUSION

In this paper, we have presented a numerical technique for determining the location of a crack in a slender beam of varying cross-section given the first three natural frequencies of the cracked beam. Sample results for a stepped beam and a two-section tapered beam are presented. This approach mimics the semi-analytical approach using the Frobenius method. The results are sufficiently accurate.

The numerical approach has several advantages over the semi-analytical approach. The method is general enough to model different variations in the depth of the beam (such as tapers, steps, or curves) without the need for a different formulation. Also, no quadruple precision calculations are needed as in the case of the semi-analytical method.

Some comments are in order over the use of this approach for crack detection. First, this method makes the same assumptions as the semi-analytical method and hence will have the same limitations. For example, since beam theory is used in the formulation, this approach will not be accurate in case of short beams. If the forward problem of determination of natural frequencies, given the location and size of the crack, cannot be solved accurately, the inverse problem solution will also be inaccurate. For example, in any real-life situation, the analytical or numerical model will predict frequencies that are different from the experimentally measured quantities. Zero setting attempts to correct this discrepancy, but zero setting is nothing more than a scaling and cannot account for all modelling or experimental errors. For example, if the three K versus β curves appear to intersect at two

different locations, we will have to go for measurement of the fourth natural frequency and solving the inverse problem with that as an additional input. However, the errors are likely to increase for the fourth natural frequency.

REFERENCES

1. B. P. NANDWANA and S. K. MAITI 1997 *Journal of Sound and Vibration* **203**, 435–446. Detection of the location and size of a crack in stepped cantilever beams based on measurements of natural frequencies.
2. T. D. CHAUDHARI and S. K. MAITI 2000 *International Journal of Solids and Structures* **37**, 761–779. A study of vibration of geometrically segmented beams with and without crack.
3. S. NAGULESWARAN 1994 *Journal of Sound and Vibration* **172**, 289–304. A direct solution for the transverse vibration of Euler–Bernoulli wedge and cone beams.
4. W. MCGUIRE and R. H. GALLAGHER 1979 *Matrix Structural Analysis*. New York: Wiley.
5. R. D. COOK, D. S. MALKUS and M. E. PLESHA 1989 *Concepts and Applications of Finite Element Analysis*. Third edition. New York: Wiley.
6. G. H. GOLUB and C. F. VAN LOAN 1989 *Matrix Computations*. Baltimore: Johns Hopkins University Press; Second Edition.
7. R. D. ADAMS, P. CAWLEY, C. J. PYE and B. J. STONE 1978 *Journal of Mechanical Engineering Science* **20**, 93–100. A vibration technique for non-destructively assessing the integrity of structures.